Study of light and heavy impurities transport in OH and ECRH plasmas on the T-10 tokamak

M.R. Nurgaliev[1], V.A. Krupin[1], L.A. Klyuchnikov[1], A.R. Nemets[1], I.A. Zemtsov[1], A.Yu. Dnestrovskij[1], D.V. Sarychev[1], V.S. Lisitsa[1], V.A. Shurygin[1], D.S. Leontiev[1], A.A. Borschegovskij[1], S.A Grashin[1], D.V. Ryjakov[1], D.S. Sergeev[1], N.A. Mustafin[1], V.M. Trukhin[1], S.N. Tugarinov[1], N.N. Naumenko[2]

[1] National Research Centre "Kurchatov Institute", Moscow, Russia

[2] B.I. Stepanov Institute of physics NASB, Minsk, Republic of Belarus

E-mail contact of main author: maxim.nurgaliev@gmail.com

Abstract. First experimental results of tungsten transport investigation in OH and ECRH plasmas of the T-10 tokamak with W-limiter and movable Li-limiter are presented in this paper. It is shown that tungsten tends to accumulate (a joint process of cumulation and peaking) near the plasma axis in ohmic regimes. Accumulation of W is enhanced in discharges with high values of a parameter $\gamma = \bar{n}_e \cdot \bar{Z}_{eff} \cdot I_{pl}^{-1.5}$ that corresponds to accumulation conditions of light and medium impurities in T-10 plasmas. Li-limiter insertion leads to a vanishing of light impurities in plasma, and besides, lithium nuclei are presented in plasma at immeasurably level (0.3-0.5% of n_e) due to the low inflow of Li with respect to other light impurities. In discharges with lithized walls values of $Z_{eff} \approx 1$ are obtained and tungsten density in the plasma center decreases by 15 to 20 times with the reduction of W inflow only by 2 to 4 times. In lithized discharges with high γ complete flattening of tungsten density profiles occurs and its central concentration decreases up to 10 times during the central ECRH. This effect is observed with the increase of the W inflow by 3 to 4 times at the ECRH stage.

1. Introduction

Impurity transport investigation in OH and ECRH plasmas have been performing on the T-10 tokamak during a long time. Dependencies of an anomalous transport coefficients profiles on plasma parameters were obtained by Ar and K injection in experiments on T-10 [1, 2]. The confinement time, which was determined by the decay of potassium Li-like VUV-line, increases linearly with the growth of a parameter $\gamma = \bar{n}_e \cdot \bar{Z}_{eff} \cdot I_{pl}^{-1.5}$, where $\bar{n}_e$ and $\bar{Z}_{eff}$ are line averaged electron density in m^{-3} and effective ionic charge respectively, I_{pl} – plasma current in kA. In these experiments, the following dependencies of anomalous diffusion D_{an} and pinch velocity V_{an} were obtained:

$$D_{an}(r) = 9 \cdot 10^{-4} \frac{I_{pl}^{1.5}}{n_e(r) \cdot Z_{eff}(r)} \propto \frac{1}{\gamma}, \quad V_{an}(r) = D_{an}(r) \frac{\nabla n_e(r)}{n_e(r)}, \qquad (1)$$

where D_{an} in m^2/s, I_{pl} in kA, n_e in 10^{19} m^{-3}. The same dependencies of balance confinement properties on γ are observed in intrinsic impurities C and O [3]. Therefore, more pronounced accumulation should be expected in discharges with high γ, which also has high values of β_I and τ_E, that causes special attention to this type of ohmic regimes.

Auxiliary ECR heating leads to the removal of light impurities [3, 4] on T-10. It was shown [3] that the ECRH removal efficiency from the plasma center is significantly determined by initial ohmic parameters characterized by γ. During the ECRH an increase of anomalous transport

coefficients occurs that results in flattening of impurity and electron density profiles. Similar effects are also observed in medium impurities on other tokamaks (see, for example, [5, 6]).

The current work is an extension of impurity transport research on T-10 and aimed to show the applicability of the dependencies obtained earlier to describe the tungsten transport. The first of all, concern with tungsten is caused by it perspective to use as a material of plasma facing components (PFCs) for ITER divertor. However, the tungsten accumulation in the plasma center is widely observed [7-9]. It can be a serious issue due to a high emissivity of W ions. In order to solve this problem a possibility of the W inflow reduction by means of the covering W-limiter via lithium together with tungsten ECRH removal is investigated in this work.

2. Experimental setup

The T-10 tokamak is a circle-shape machine with a rail and a circle limiters and following parameters: major radius R=1.5 m, minor radius a=0.3 m, toroidal magnetic field $B_t \leq 2.5$ T, plasma current $I_{pl} \leq 350$ kA, line averaged density $\bar{n}_e$ =0.5-7·10^{19} m^{-3}, ECR heating power $P_{EC} \leq 3$ MW. During the experimental campaign 2015-2016 carbon rail and circle limiters were replaced by tungsten ones. Movable Li-limiter was also installed [10].

Electron density profile $n_e(r)$ measurements are performed via 16-channel interferometer. ECE diagnostics is used for measurements of electron temperature profiles $T_e(r)$. Values of $T_e(0)$ are also determined by the slope of the spectrum in the SXR-region. The CXRS diagnostics of T-10 [11] is used for measurements of ion temperature profiles $T_i(r)$ and light impurity concentration. $Z_{eff}(r)$ profiles are measured independently via bremsstrahlung diagnostic complex [12].

W density profiles are determined by means of total radiation losses that is registered by 16-channel grids of collimated AXUV-detectors. AXUV detectors register the radiation of total line emission in energy range from approximately 50 eV to 10 keV in whole bulk plasma. The tungsten inflow into the plasma is estimated by emission of WI 4008 Å line measured via central line of sight (LOS) on the inner part of circle W-limiter.

3. Determination of W density in T-10 experiments

3.1 Tungsten behaviour in ohmic regimes

The basis for the integral emission profiles application for studying tungsten transport properties is a location of fractional abundance of W-ion $f_W^Z = n_W^Z / \sum n_W^Z$ on coronal radii. This fact was demonstrated in work from ASDEX Upgrade [13] where preservation of coronal equilibrium even at tenfold magnification of neoclassical transport is shown. Coronal positions of f_W^Z can be realized due to shorter times of atomic processes than transport times. T-10 has faster transport and slower atomic processes because of smaller size and lower T_e than AUG. Therefore, the validation of the f_W^Z coronal equilibrium preservation has to be performed in T-10 conditions. For this purpose, distributions of W ions in plasma are calculated with atomic rate coefficients [14] for coronal and transport cases. Transport calculations are performed in STRAHL code [15] including neoclassical and anomalous transport (1).

As it is shown in FIG.1 the coronal equilibrium of f_W^Z remains in typical OH discharges with $T_e(0)$=1 keV, as well as in ECRH regimes with $T_e(0)$=3 keV and increased W transport. Note that the increase of transport does not lead to a substantial displacement of W fractional

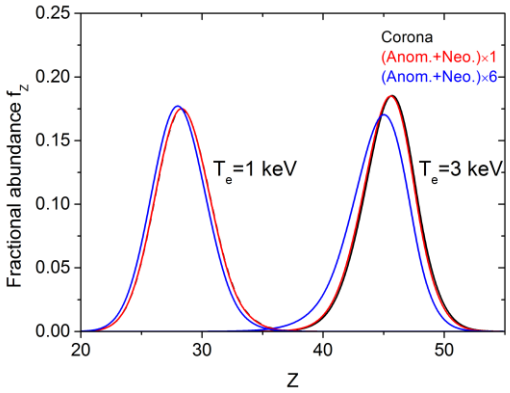

FIG. 1. Fractional abundance distributions of tungsten and transport influence on it

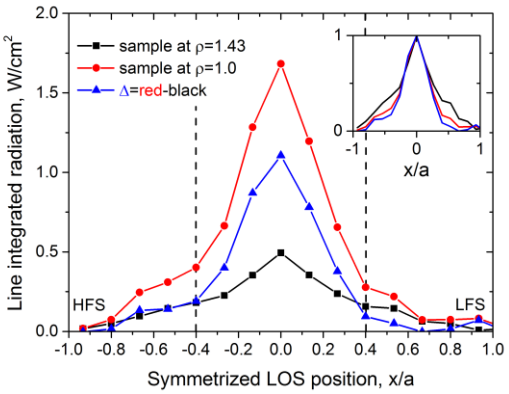

FIG. 2. LOS-integrated profiles of total radiation losses measured by AXUV in saw-teeth free discharges, small picture -- normalized profiles

abundance from its coronal positions. Thereby total tungsten density $n_W = \sum n_W^Z$ can be determined from:

$$P_{rad} = n_W n_e L_W^{eff}, \qquad (2)$$

where P_{rad} is W total radiation power density in W/m^3, L_W^{eff} is effective cooling factor for tungsten ions in coronal equilibrium in W·m^3. In the current paper $L_W^{eff}(T_e)$ calculated by method of local plasma frequency [16] are used to estimate tungsten density profiles (marked as "LPF" in figure 9 in [16]).

3.2 Determination of W emission localization zone

In order to use AXUV diagnostic it is important to determine how reliable tungsten radiation stands out from the total emission of all impurities and where it is located. For this purpose, W-sample (a copy of the rail limiter tile) is inserted into the plasma on radius $\rho=r/a \sim 1$. Surface of the sample heats during the couple of discharges to temperatures close to the melting point that result in growth of total W inflow into the plasma.

As it can be seen in FIG.2 tungsten sample insertion is accompanied by the strong increase of emission from plasma center ($\rho \le 0.4$). The observed difference between the radiation losses profiles with and without sample allows estimating the localization zone of W ions emission. Size of this zone is $|\rho| \le 0.4$ to 0.5 for discharges with I_{pl}=180 kA, $\bar{n}_e$ =4.3·10^{19} m^{-3}. As it is shown below, intense tungsten accumulation occurs exactly in this area. It is necessary to note that LOS-integrated profiles of AXUV with inserted sample, without it, as well as differencing profile are similar inside the mentioned zone (FIG.2 right-top). This fact indicates the predominance of tungsten emission over the emission of other possible impurities (Fe, Cu, Mo et.al.) in T-10 plasma center.

4. Experimental results and its analysis

4.1. Tungsten behaviour in ohmic regimes

4.1.2 Comparison of W and light impurities transport properties

Tungsten expectedly tends to accumulate in the plasma center in T-10 OH discharges. The process of accumulation is enhanced in discharges with high values of γ parameter, i.e. in discharges with low current and high density. The increase of γ during a discharge, for example due to electron density growth, results in following related effects: intense accumulation and

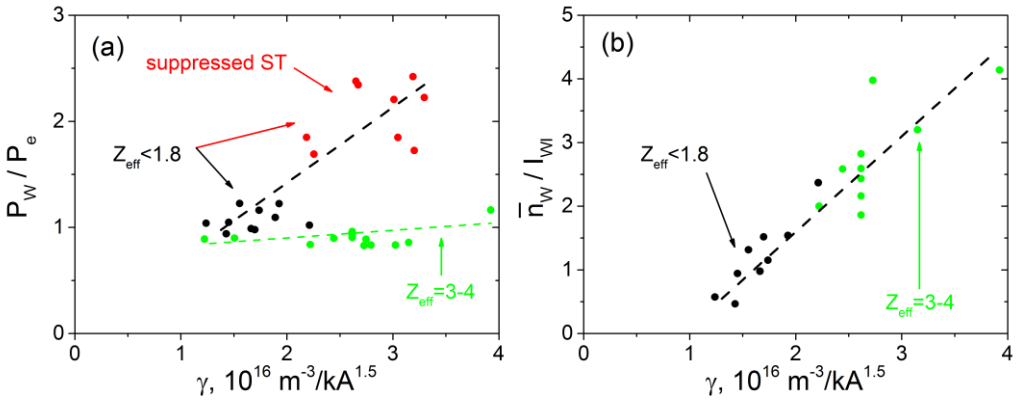

FIG. 3. The dependence of tungsten accumulation on γ: (a) P_W relative to peaking of electrons P_e; (b) Cumulation $\bar{n}_W / I_{WI}$

saw-tooth oscillations suppression. The latter could be caused by radiative cooling of central zone due to W ions emission and current density flattening.

In this work, we are trying to link tungsten transport properties to parameter γ analogous to transport of medium [2] and light [3] impurities on T-10. The W accumulation is considered here as a result of two processes: tungsten cumulation (W density increase without its profile changes) and peaking of W density profile relative to electrons. Peaking level is characterized by peaking factor $P_W = n_W(0) / \bar{n}_W$ and cumulation level – as $\bar{n}_W / I_{WI}$, where $n_W(0)$ is the central W density, $\bar{n}_W$ is line averaged W density inside $\rho \leq 0.5$, I_{WI} is brightness of WI 4008 Å line.

It can be seen from FIG.3 the peaking factor and the tungsten cumulation generally increase with growth of γ that is not contrary to corresponding dependencies of light and medium impurities in T-10 plasma. However, in case of contaminated plasma with Z_{eff}=3-4 peaking factor P_W has slight dependence on γ due to neoclassical pinch attenuation in plasma with high level of C and O nuclei density. The different dependence of the W peaking factors on γ in pure and contaminated plasmas distinguishes tungsten from light impurities. It could be explained by the improvement of tungsten confinement properties with γ growth due to neoclassical transport increase while of light – due to anomalous decrease.

4.1.3 Gas puffing influence on W accumulation process in lithized discharges

The process of the tungsten accumulation can be simply controlled in discharges with lithized walls by deuterium gas puffing. It can be performed because of a vanishing of peripheral radiative layer created by light impurities due to the drastically reduced inflow of C and O. In FIG.4 time evolution of plasma parameters after the abrupt switching-off gas puff are demonstrated. In the first ≈50 ms peaking of $n_e(r)$ [17] and radiation losses profiles occurs. Deuteron density $n_d(r)$ peaks together with $n_e(r)$ in plasma with Z_{eff}≈1. The peaking of electron density leads to the anomalous pinch enhancement $V_{an} / D_{an} \approx \nabla n_e / n_e$ while peaking of deuterons – to the increase of neoclassical pinch V_{neo}^Z (3). Moreover, observed broadening of ion temperature $T_i(r)$ (FIG.5b) causes the impurities temperature screening decrease [18]:

$$\frac{V_{neo}^Z}{D_{neo}^Z} = \frac{Z}{Z_d}\left(\frac{\nabla n_d}{n_d} + \frac{H}{K}\frac{\nabla T_i}{T_i}\right) \qquad (3)$$

where D_{neo}^Z is neoclassical diffusion coefficient with charge Z, Z_d=1 is deuteron charge, H and K are functions of $n_Z Z^2 / n_d Z_d^2$ and ion collisionality ν_d^*, usually the ratio H/K is negative for T-10 plasma. Electron temperature profile $T_e(r)$ becomes broader after the switching-off gas puff and loop voltage decreases that confirms of peripheral T_e growth (FIG.4b).

As a result of all stated processes, the intense accumulation of tungsten appears in plasma. Apparently, T_e profile broadening after switching-off the gas puff and due to the rise of W radiation in the center leads to current density profile flattening and consequently saw-tooth activity suppression. Furthermore, higher peripheral temperature should contribute to an increase of W inflow into the plasma. However, no increase of WI emission is observed that can be explained by covering W-limiter via lithium.

The gas puff recovery initiates a tungsten de-accumulation process (see FIG.5a) which is accompanied by strictly inverse changes of n_e, T_e, T_i and restoration of saw-tooth oscillations. Herewith, WI line emission drops to almost zero level (FIG.5b). In this case, on T-10, as well as on JET [19], a noticeable decrease of W inflow is observed after switching-on deuterium gas puff.

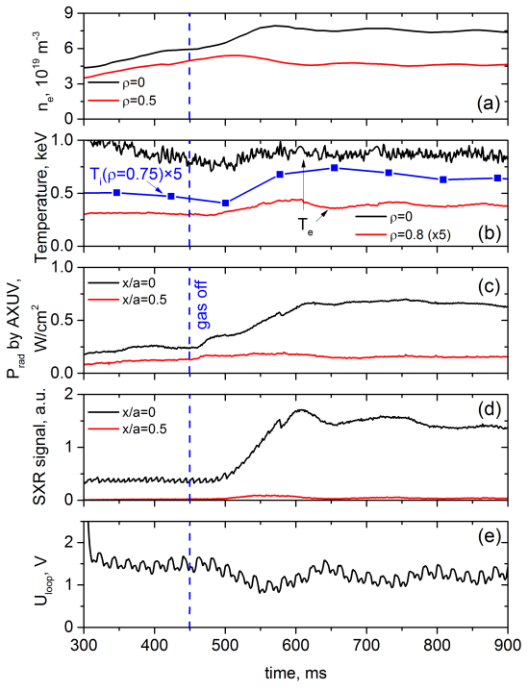

FIG. 4. The influence of switching-off gas puff on W accumulation process in discharge 67983 (I_{pl}=180 kA, $\bar{n}_e$ =4.5·10^{19}m^{-3})

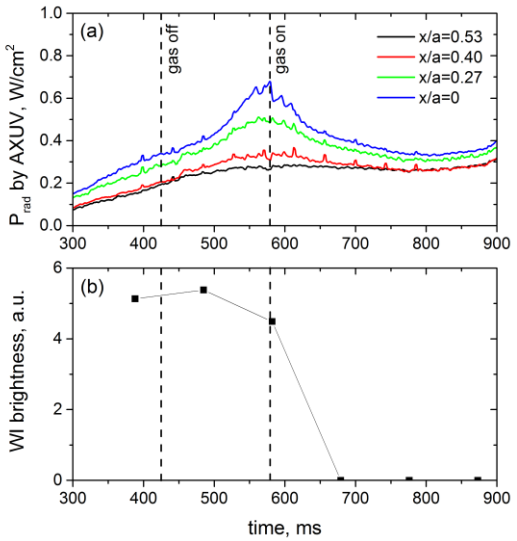

FIG. 5. The disruption of tungsten accumulation process by gas modulation in discharge 68076 (I_{pl}=250 kA, $\bar{n}_e$ =6.7·10^{19}m^{-3})

4.1.4 Differences of tungsten accumulation processes in high- and low-Z_{eff} plasmas

In plasma with lithized walls and Z_{eff}≈1 tungsten cumulates weaker than in plasma with Z_{eff}=3-4 (FIG.3b). As it is show in FIG.6 significant (more than 10 times) reduction of central tungsten density occurs while W inflow estimated by WI emission decreases only by 2 to 4 times. This tungsten behaviour can be explained by reduction of anomalous transport in accordance with (1) and attenuation of neoclassical transport in low collisionality plasma with Z_{eff}≈1 in comparison with plasma with Z_{eff}=3-4. In its turn, the γ parameter reflects the ratio of the anomalous and neoclassical transport. Therefore, γ can characterize W, light and medium impurities transport.

4.2. Features of Li-limiter on T-10

As it is shown in FIG.6 W accumulation is weaker in discharges with lithized walls and Z_{eff}≈1. Achieving of Z_{eff}≈1 values is confirmed by measurements of effective ionic charge via bremsstrahlung diagnostics. The CXRS diagnostics demonstrate significant changes of light impurities density after lithization: C (4 %→0.3 %), N (0.4 %→0.1 %) and O (3%→<0.1%).

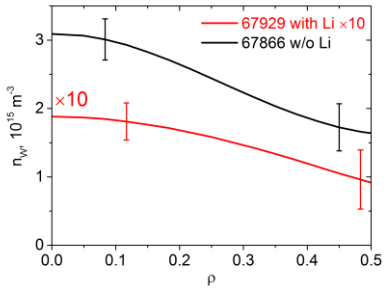

FIG. 6. n_W profiles in lithized and non-lithized discharges

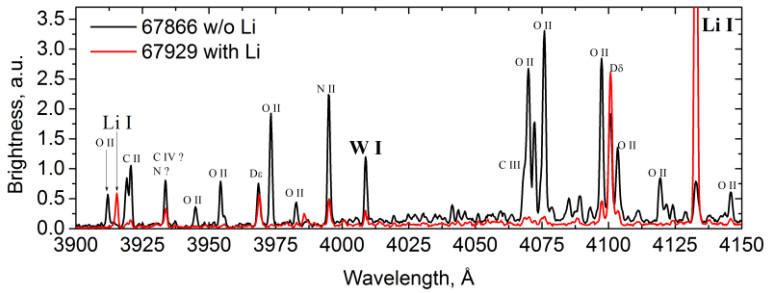

FIG. 7. Spectra near 4008 Å in lithized and non-lithized discharges

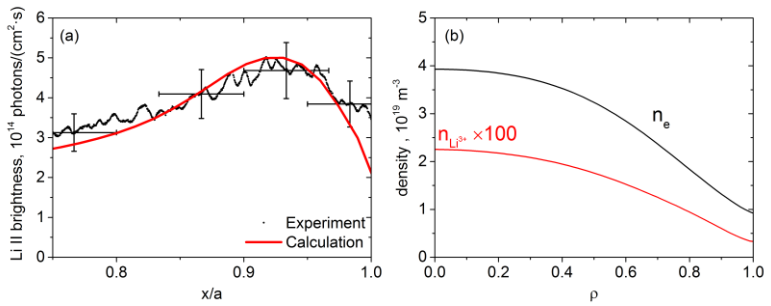

FIG. 8. Simulation of lithium in STRAHL code: (a) LOS-integrated Li II 5485 Å brightness; (b) Li^{3+} and electron densities

The main reason of light impurity content reduction is the strong decrease of its inflow into the plasma as it is possible to see in FIG.7. Such high gettering efficiency of Li-limiter on T-10 is determined by its location in region with the most intense recycling processes, i.e. in the same poloidal cross-section as the W-limiter. Densities of impurity atoms and molecules are much higher (30-100 times) in this region than the average in whole of plasma.

Reduction of WI 4008 Å emission is also observed after the lithization (FIG.7), despite the increase of T_e and T_i on plasma periphery. This effect can be related to the covering W-limiter by lithium as it is mentioned above. Note that inflow of lithium atoms into the plasma arising from the lithized walls does not lead to an appearance of Li nuclei in the plasma on a measurable level of the T-10 CXSR diagnostics (0.3% of n_e). The reason of the low level of Li^{3+} is a small Li inflow. As it is possible to see in FIG.8a, LOS-integrated profile of LiII 5485 Å line calculated in code STRAHL with (1) and neoclassical transport is in good agreement with the measured one. Description of LiII emission in absolute values allows determination the values of Li atoms inflow $5.5 \cdot 10^{17}$ $m^{-2} \cdot s^{-1}$, which explains low level of Li^{3+} in the plasma center FIG.8b. Therefore, modeling explains why there is no measurable CXSR-signal in LiIII 5167 Å spectra in discharges with lithized walls.

What is important is the absence of measurable Li^{3+} density even at the ECRH regimes with power up to 2 MW. Herewith, an increase of 1.5–3 times of emission of Li^{1+} ions is observed during ECRH that indicates Li inflow increase. Nevertheless, the ECRH removal not only offsets the growth of impurity source but also results in light impurities nuclei decrease in the plasma center relative to initial ohmic level as it is shown in [4] on T-10. Further, it would helpful to understand why Li atom inflow is much lower than inflow of C, N and O in non-lithized discharges. A reason could be not only in a low recycling coefficient but also in an inability of Li to form volatile compounds unlike C, N and O.

4.3. ECRH regime

As it is mentioned above, the ECR heating input leads to the particle confinement degradation. The rise of anomalous transport coefficients, neoclassical accumulation decay and flattening of impurities density concentration are observed. The most notable effect of impurities removal from the center is caused by central ECRH [5], so only this type of auxiliary heating is considered in this paper.

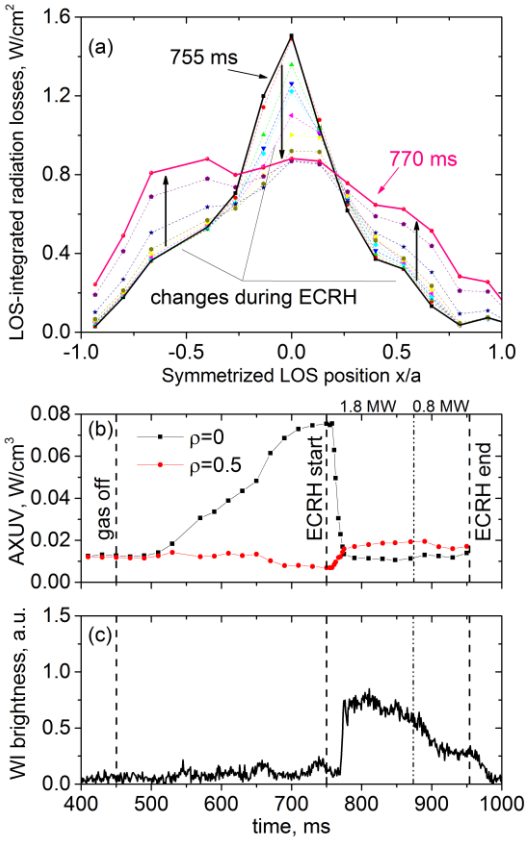

FIG. 9. Changes of total radiation losses profile during ECRH in discharge 68086 (I_{pl}=220 kA, $\bar{n}_e$ =4.5·10^{19}m^{-3}): (a) flattening of LOS-integrated AXUV profiles; (b) dynamics of radiation losses; (c) dynamics of WI emission

Changes of LOS-integrated radiation losses profiles measured by AXUV during the ECRH are shown in FIG.9a. The rapid decrease of radiation in the center and its growth at the periphery occurs. Hollow radiation losses profiles are observed as it is shown in FIG.9b. Tungsten removal process proceeds together with the increase of WI emission that indicates the growth of W inflow on the circle limiter during the ECRH.

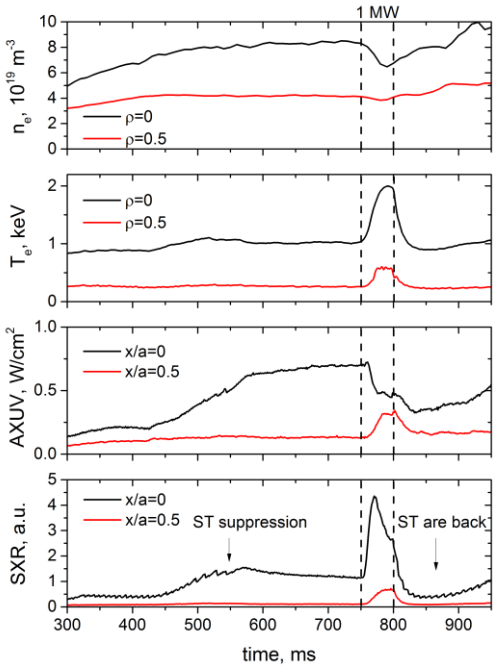

FIG. 10. Fast tungsten removal by short ECRH results in saw-tooth oscillations retrieval in discharge 68037 (I_{pl}=180 kA, $\bar{n}_e$ =3.9·10^{19}m^{-3})

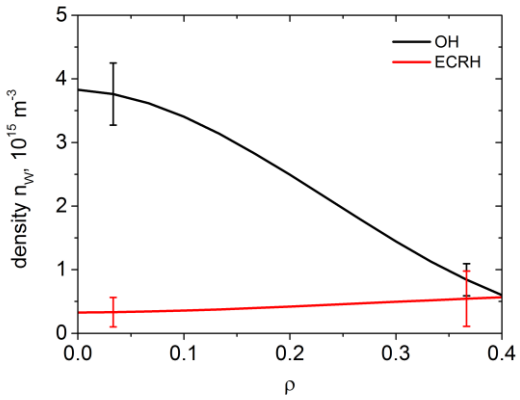

FIG. 11. Change of tungsten density profile in OH-ECRH transition in discharge 67986 (I_{pl}=180 kA, $\bar{n}_e$ =4.7·10^{19}m^{-3} P_{EC}=1 MW)

As it is possible to see by time evolution of central AXUV LOS (see FIG.10), the W removal in discharge with P_{EC}=1 MW is close to discharge with P_{EC}=1.8 MW (in FIG.9a) and corresponds to power increase as $P_{EC}^{0.5}$. Herewith, the radial AXUV profile changes drastically what is determined mainly by W removal and far less by n_e and T_e variation. The removal in FIG.10 occurs at the saw-teeth free stage of discharge and the ECRH does not lead to an increase of saw-tooth activity. It indicates that the removal is produced principally by the rise of anomalous transport rather than saw-tooth oscillations.

A comparison of W density profiles at the OH and ECRH stages are shown in FIG.11. One can see that tungsten density drops off by ≈10 times and $n_W(r)$ flattens. Taking into account the increase of W inflow by 3 to 4 times, W ECRH removal efficiency from plasma center is about 30–40 while for light impurities this ratio is about 10–20 [3]. Therefore, tungsten is removed from plasma is more efficient than light impurities even considering the spread of known $L_W^{eff}(T_e)$ dependencies.

5. Conclusion

First experimental results of the tungsten transport investigation in the OH end ECRH plasmas are obtained. Tungsten, as expected, accumulates (peaks and cumulates) in plasma center in T-10 ohmic discharges. It is shown that peaking and cumulation levels increase with growth of $\gamma = \bar{n}_e \cdot \bar{Z}_{eff} \cdot I_{pl}^{-1.5}$ parameter. Thereby, in ohmic regimes of T-10 similar dependencies of light, medium and heavy impurities confinement on γ are observed. However, investigations that are more systematic are required for further details.

In T-10 conditions W are efficiently removed from plasma by wall lithization due to the reduction of W inflow by 2 to 4 times and also leads to the decrease of W penetration ability due to low collisionality of plasma with $Z_{eff}\approx1$. The strong W accumulation is observed in high–β_I and –τ_E discharges, which corresponds to the highest values of γ. In plasma with $Z_{eff}\approx1$ it is possible to stimulate the tungsten accumulation process by the switching-off gas puffing and by switching it on – to suppress this process.

It is necessary to note that low level of lithium nuclei density is observed in plasma with lithized walls what can be explained by extremely low Li atoms inflow $5.5\cdot10^{17}$ $m^{-2}\cdot s^{-1}$ into the plasma.

Tungsten density profile flattens and the central density reduces during the central ECRH. This reduction can be up to 10 times in discharges with the highest ohmic accumulation. Taking into account the rise of W source by 3 to 4 times at the ECRH stage it can be concluded that W removal is more pronounced than the same effect of light impurities.

Acknowledgment

Authors are grateful to Dr. R. Dux for providing STRAHL code and advices on its usage. The work is carried out by the funding of Russian Science Foundation Project No. 14-22-00193.

References

[1] KRUPIN, V. et al., Sov. J. Plasma Physics 9 (1983) 529
[2] KRUPIN, V. et al., in 12th EPS Conference on Plasma Physics, pages 207–210, Budapest, 1985.
[3] NURGALIEV, M. et al., in 43rd EPS Conference on Plasma Physics, Leuven, 2016, P2.069.
[4] KLYUCHNIKOV, L. et al., in 25th IAEA FEC, St. Petersburg, 2014, EX/P1–44.
[5] SERTOLI, M. et al., Plasma Physics and Controlled Fusion 53 (2011) 035024.
[6] HONG, J. et al., Nuclear Fusion 55 (2015).
[7] ARUNASALAM, V. et al., in 8th EPS Conference on Plasma Physics, pages 17–28, Prague, 1977.
[8] NEU, R. et al., Journal of Nuclear Materials 438 (2013) S34
[9] ANGIONI, C. et al., Nuclear Fusion 54 (2014) 083028.
[10] SARYCHEV, D. et al., in 26th IAEA Fusion Energy Conference, Kyoto, 2016, OV/4-5
[11] KLYUCHNIKOV, L. A. et al., Review of Scientific Instruments 87 (2016) 053506.
[12] KRUPIN, V. A. et al., Problems of atom. Sci. and Techn. ser. Thermonuclear fusion 39 (2016) 81.
[13] PÜTTERICH, T. et al., Plasma Physics and Controlled Fusion 50 (2008) 085016.
[14] ASMUSSEN, K. et al., Nuclear Fusion 38 (1998) 967.
[15] DUX, R., STRAHL User Manual, Technical Report IPP 10/30, IPP Max-PlanckIstitut für Plasmaphysik, 2006.
[16] DEMURA, A. et al., Atoms 3 (2015) 162.
[17] VERSHKOV, V. A. et al., Nuclear Fusion 39 (1999) 1775.
[18] WENZEL, K. et al., Nuclear Fusion 30 (1990) 1117.
[19] FEDORCZAK, N. et al., Journal of Nuclear Materials 463 (2015) 85.